Hindawi Publishing Corporation
EURASIP Journal on Image and Video Processing
Volume 2008, Article ID 542378, 19 pages
doi:10.1155/2008/542378

Research Article

Fuzzy Mode Enhancement and Detection for Color Image Segmentation

Olivier Losson, Claudine Botte-Lecocq, and Ludovic Macaire

Laboratoire LAGIS (CNRS UMR 8146), Université des Sciences et Technologies de Lille, Bâtiment P2, Cité Scientifique, 59655 Villeneuve d'Ascq Cédex, France

Correspondence should be addressed to Olivier Losson, olivier.losson@univ-lille.fr

Received 20 July 2007; Revised 30 November 2007; Accepted 27 January 2008

Recommended by Konstantinos Plataniotis

This work lies within the scope of color image segmentation by pixel classification. The classes of pixels are constructed by detecting the modes of the spatial-color compactness function, which characterizes the image by taking into account both the distribution of colors in the color space and their spatial location in the image plane. A fuzzy transformation of this function is performed, based on fuzzy morphological operators specifically designed for mode detection. Experimental segmentation results, using several synthetic and benchmark images, show the interest of the proposed method.

1. INTRODUCTION

Color image segmentation consists in partitioning the pixels of an image into separate regions, which are groups of connected pixels with homogeneous color properties. Among low-level image processing tasks, segmentation is one of the most challenging and addressed issues. Indeed, this step is crucial in many applications requiring region and object identification in the scene, as in content-based image retrieval schemes, object-based video coding, and so on. Color image segmentation is classically achieved by an analysis of either the image plane or a color space.

Image plane analysis methods can be divided into two major categories. The boundary-based methods look for discontinuities in the image to detect edge pixels [1, 2]. They often require time-consuming postprocessing tasks, such as edge tracking, to yield closed object boundaries. Conversely, region-based techniques assume that neighboring pixels belonging to the same region share similar color properties. Region growing procedures start from selected seed pixels and iteratively aggregate all similar neighbors that respect homogeneity-based conditions [3]. They generally result in an oversegmented image, which can be processed by region merging algorithms. These algorithms usually model the image by a region adjacency graph, and then analyze such a graph in order to iteratively merge adjacent regions with similar colors [4].

Since most of the image plane analysis methods require a delicate adjustment of parameters, a lot of authors propose to globally analyze the color distribution in a color space by means of pixel classification techniques. For this purpose, each pixel is associated with a color point whose coordinates are its color component levels (e.g., red, green, and blue levels when the (R, G, B) color space is considered).

Image segmentation methods by pixel classification rely on the assumption that homogeneous regions in the image give rise to clusters of color points in the color space, each of them corresponding to a class of pixels. The key problem consists in cluster identification, based on either a clustering technique or an analysis of an underlying probability density function (pdf).

Clustering schemes aim at identifying the gravity centers of clusters thanks to dedicated metrics in the color space [5], such as the Euclidean distance used by a competitive learning scheme [6] or a fuzzy metric used by the fuzzy C-means method [7]. Consequently, most of these schemes make strong assumptions about the cluster shapes. When the distributions of the color points are neither globular nor compact, these clustering techniques tend to fail in constructing pixel classes which correspond to the actual regions in the image.

In order to avoid this problem, several authors propose to analyze the underlying pdf of all the colors occurring in the image. This function can be directly approximated by the 3D color histogram. Each bin, whose coordinates in the histogram are the component levels of a given color, is valued with the number of pixels having the corresponding color in the image. Cluster identification is achieved by detecting the domains of the color space with a high density of points (i.e., the domains—called *modes*—where the pdf reaches high values). The pixels whose colors are located in these modes define the prototypes of the classes. The remaining unlabeled pixels are finally assigned to one of these classes according to a decision rule. In that way, the constructed regions of the segmented image are composed of the connected pixels assigned to the same classes.

As far as color image segmentation is primarily viewed as a mode detection problem, local maximums of the pdf may be seen as peaks, whereas low values of the pdf may be considered as valleys. This topographic point of view enables to exploit techniques such as watershed-based methods [8]. Originally applied to a gradient image, the algorithm using immersion [9] has been run on the additive inverse histogram [10]. Nonetheless, it still provides oversegmented images and therefore requires a mode merging step [11], even in user-assisted schemes [12]. Hill climbing has also been investigated, but this approach is subject to loss of details. Therefore, it requires histogram peak manipulations to avoid that small yet significant peaks get merged with larger ones [13].

Zhang et al. propose to detect valleys of the pdf, instead of modes, by examining the normalized density derivative of the pdf [14]. The underlying hypothesis is that there is no abrupt change in density between two adjacent colors that belong to the same mode. A final convexity test is performed to improve the robustness of the procedure when the color distributions highly overlap in the color space.

Most of pixel classification schemes are designed to identify either globular or ellipsoidal clusters of color points, or modes which are well separated by valleys of the pdf. Unfortunately, those strong assumptions are not always verified, especially for real noisy natural images when the objects of the observed scene are illuminated with a spatially nonuniform lighting. That explains why a lot of color image segmentation methods by pixel classification fail in distinguishing the objects when the lighting intensity varies all over the scene. The issue tackled here is related to the construction of pixel classes thanks to mode detection when the color distributions of the distinct regions to be retrieved are nonglobular.

In Section 2, we focus on the specific problem of color image segmentation in case of nonuniform lighting. In Section 3, we introduce the spatial-color compactness function characterizing a color image. Then, we detail the key point of this paper, namely how to detect the modes of this function by means of a specific fuzzy morphological transformation in Section 4. Experimental results are provided in Section 5 in order to assess the effectiveness of our fuzzy mode detection scheme for color image segmentation. Finally, a conclusion is made in Section 6.

2. IMAGE SEGMENTATION AND NONUNIFORM LIGHTING

2.1. Illustrative example

Let us consider the simple case of a scene composed of two distinct one-colored objects, the reflectance properties of each object being identical all over its surface. So, when the surface of each object is illuminated by a uniform lighting, the colors of pixels representing it are identical. Because of the Gaussian acquisition noise, colors give rise to clusters which, depending on their overlapping degree, can be more or less easily identified by clustering methods designed for image segmentation.

When the lighting intensity gradually varies all over the object surface, the (R, G, B) color components of the pixels vary too. As an example, the synthetic image in Figure 1(a) is made of two rectangular surfaces illuminated by a lighting whose intensity increases with respect to the pixel row coordinates. In order to simplify the illustration, the blue component has been set to zero all over the image, as for all the synthetic images used in this paper. Figure 1(b) shows the histogram $H(R, G)$ of this image where R and G are the color components of each pixel. Since the reflectance properties are identical all over the surface of each object and since there is no acquisition noise, the colors of the two surfaces give rise to two diagonal linear modes of the histogram in the (R, G) chromatic plane.

In order to take into account the acquisition noise, this image is corrupted by a noncorrelated Gaussian noise, with a standard deviation equal to 10, which is independently added to each color component (see noisy synthetic image in Figure 2(a)). Figure 2(b) shows that, since the distributions of these colors highly overlap, the two modes are not well separated by a valley. Therefore, they are hardly detectable by an automatic processing of this histogram. This is essentially due to the fact that the histogram only considers the colors of the pixels and ignores their spatial location in the image. So, in case of nonuniform lighting, the histogram is not always a relevant tool for color image segmentation by mode detection.

2.2. Spatial-color pixel classification

Spatial-color pixel classification approaches take into account both the distribution and the spatial location of the colors to segment the image. This family of recent methods can be divided into two groups: the techniques which apply a clustering procedure followed by a spatial analysis, and those which detect the modes by analyzing spatial-color functions describing the image.

Ye et al. apply the clustering algorithm called DBSCAN to image segmentation [15]. First, this scheme identifies *core* pixels, namely pixels surrounded by a minimum number of neighbors with similar colors. The similarity is ensured if the colors of the considered pixels are located in an ellipsoid of the (H, V, C) color space. Then, the procedure regroups pixels which are density-reachable from those detected core pixels.

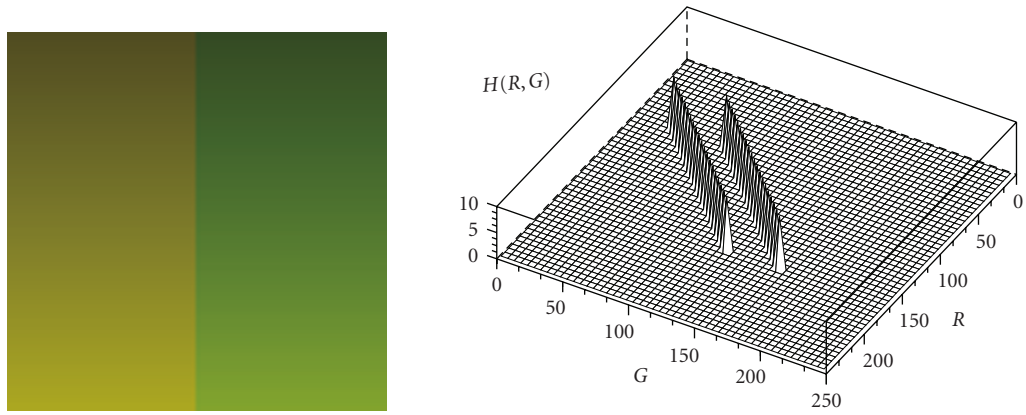

(a) Synthetic image (b) Histogram in the (R, G) plane

FIGURE 1: Synthetic image of two surfaces illuminated by a spatially nonuniform lighting intensity.

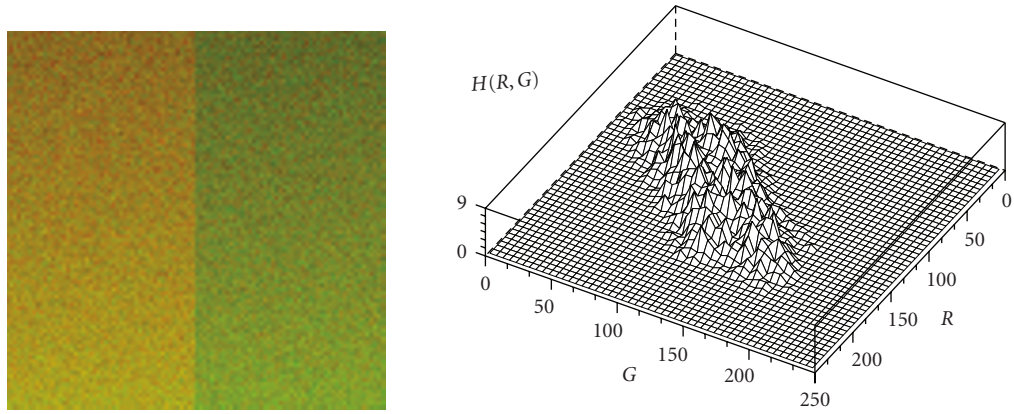

(a) Noisy synthetic image (b) Histogram in the (R, G) plane

FIGURE 2: Synthetic image, corrupted by acquisition noise, of two surfaces illuminated by a spatially nonuniform lighting intensity.

JSEG is one of the most well-known segmentation algorithms which achieve a clustering step followed by a spatial analysis [16]. A first step of color quantization yields an image of labels called *class-map*. Considering the class-map as a special color-texture composition, the proposed J measure relies on the dispersion of the locations of the prototype pixels to provide a "good" segmentation criterion. The local homogeneity measure J, computed on a neighborhood of a given size, is all the higher as the center pixel likely belongs to a region boundary. Using the J criterion, a region merging procedure is finally applied to the class-map in order to avoid oversegmentation. Wang et al. [17] show that the hard classification caused by the color quantization step both degrades the flexibility of JSEG and, subsequently, tends to split the image areas with smooth color transitions into several classes. Figure 3(a), which shows the JSEG segmentation of the synthetic image in Figure 2(a), illustrates this phenomenon. In this image, as in the following segmented ones, the edges of the reconstructed regions are white marked. This segmentation result is provided by the software implementing JSEG, available on the web site http://vision.ece.ucsb.edu/segmentation/jseg/, and configured with the default parameter values suggested by the authors. Wang et al. argue and illustrate on a simple example that the J measure, being applied to a class-map, fails to give the boundary strength and hence does not allow to distinguish regions with similar distributions of textural patterns but different color contrasts [18]. JSEG is therefore prone to oversegmentation in case of spatially varying lighting. Those authors ascribe it primarily to the fact that color and spatial information are taken into account separately. Therefore, they propose to combine the textural homogeneity measure J and the color discontinuity measure H used by HSEG method [19]. This combined measure is suitable to characterize homogeneous texture regions, and to make distinguishable class-maps with strong and weak boundaries.

Comaniciu and Meer construct a spatial-color function describing the image, and propose to detect the modes by jointly considering spatial and color distributions. They apply the mean shift algorithm in the joint spatial-color space for color image segmentation [20]. The mean shift method is based on a kernel K, used by the Parzen density estimator, and on a second kernel G defined from the derivative of the

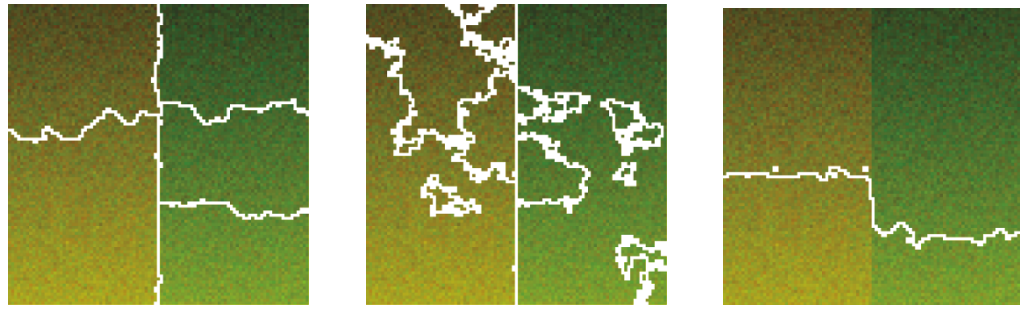

(a) JSEG [16] (b) Mean shift [20] (c) SCDA [21]

Figure 3: Segmentation results of the image in Figure 2(a) provided by well-known spatial-color pixel classification methods.

profile function of K. At a given point, the mean shift is computed as the difference between the weighted average of the neighboring observations (using G as weights), and the kernel center. For a set of points, the mean shift procedure converges towards the maximums of the underlying pdf without estimating the density. Moreover, the translation of the kernel is automatically adapted to the local density of points: low densities yield large mean shift steps. Once the stationary points have been detected in this way, a pruning procedure is necessary to retain only the local maximums and hence to retrieve the modes. After nearby modes have been pruned, each pixel is associated with a significant mode of this joint space. As shown by Figure 3(b), the EDISON software implementing the mean shift algorithm available at http://www.caip.rutgers.edu/riul/research/code/EDISON/, and run with the default parameter values suggested by the authors, provides oversegmentation in case of nonuniform lighting.

Macaire et al. [21] also integrate both color distribution and spatial location to construct the pixel classes. The selection of color domains relies on the analysis of the *spatial-color compactness degree*, which takes into account both pixel connectedness and color homogeneity. This method unfortunately requires the desired number of classes. Since it assumes globular clusters of color points, it is inappropriate for the identification of clusters with irregular shapes. As an illustration of the limits reached by this approach, hereafter referred to as SCDA, Figure 3(c) shows the corresponding segmentation result obtained when the lighting is not spatially uniform.

2.3. Our spatial-color approach

In this paper, we propose a new mode detection technique based on the analysis of the *spatial-color compactness function* (sccf) describing the color image. This function, called *compacigram* in [22], describes both the distribution of the colors in the color space and their spatial location in the image plane. It is a trivariate function whose value at each color point is a measure of the spatial-color compactness degree, introduced by Macaire et al. [21] and described in the next section. The modes to be detected are then defined as color space domains where the sccf reaches high values. They are separated by valleys, which are color space domains where the sccf has low values. A first basic mode detection procedure using convexity analysis has been applied to the sccf in order to show the interest of this describing function [22]. Nevertheless, the results of such a procedure strongly depend on the thresholds used to detect the modes. Moreover, a postprocessing step is required to preserve only the significant detected modes. In order to avoid these adjustments, we propose to perform a fuzzy morphological transformation of the sccf based on fuzzy morphological operators specially designed for mode detection (see Section 4).

3. SPATIAL-COLOR COMPACTNESS FUNCTION OF A COLOR IMAGE

A color image can be described by the spatial-color compactness function sccf, which combines the connectedness and homogeneity degrees, both introduced in [21] and briefly described in the next subsection.

3.1. Connectedness and homogeneity degrees

Let $\mathbf{C} = [C_R, C_G, C_B]^T$ be a color point in the discrete color space $\mathcal{C} = (R, G, B)$, and let $\mathcal{D}_l(\mathbf{C})$ be a cube, centered at $\mathbf{C}$ and whose edges of length l (an odd integer) are parallel to the axes of $\mathcal{C}$. The cube $\mathcal{D}_l(\mathbf{C})$ therefore includes all the color points $\mathbf{C}' = [C'_R, C'_G, C'_B]^T$ adjacent to $\mathbf{C}$, such that $C_i - (l-1)/2 \leq C'_i \leq C_i + (l-1)/2$, $i = R, G, B$. Let us consider the color image $\mathbf{I}$ where each pixel P is characterized by its color $\mathbf{I}(P)$. The subset formed by all the pixels P whose colors $\mathbf{I}(P)$ are included in the cube $\mathcal{D}_l(\mathbf{C})$ is hereafter referred to as $S_l(\mathbf{C})$.

For any color point $\mathbf{C}$ of the color space, the connectedness degree $CD_l(\mathbf{C})$ is defined as the average number of neighbors of each pixel of $S_l(\mathbf{C})$ which also belong to $S_l(\mathbf{C})$ [23]. When the pixel subset $S_l(\mathbf{C})$ is empty, $CD_l(\mathbf{C})$ is set to 0. Otherwise, by considering an $nb \times nb$ neighborhood of each pixel (nb being an odd integer, set to 3 in this paper), $CD_l(\mathbf{C})$ is defined as

$$CD_l(\mathbf{C}) = \frac{\sum_{P \in S_l(\mathbf{C})} \mathrm{Card}\{N[S_l(\mathbf{C})](P)\}}{(nb^2 - 1) \cdot \mathrm{Card}\{S_l(\mathbf{C})\}}, \quad (1)$$

where $N[S_l(\mathbf{C})](P)$ is the subset of the neighboring pixels of a pixel $P \in S_l(\mathbf{C})$, among its $(nb^2 - 1)$ neighbors, which also belong to $S_l(\mathbf{C})$. This degree ranges from 0 to 1, and a value of $CD_l(\mathbf{C})$ close to 0 indicates that the pixels of $S_l(\mathbf{C})$ are scattered in the image plane, while a value close to 1 means that most of the pixels belonging to the considered subset are connected to each other in the image.

The homogeneity degree $HD_l(\mathbf{C})$ is defined as the ratio of the average local dispersion of colors in the neighborhood of each pixel in $S_l(\mathbf{C})$, to the global color dispersion of the pixels belonging to $S_l(\mathbf{C})$. The global dispersion measure, denoted by $\sigma(S_l(\mathbf{C}))$, is estimated as

$$\sigma(S_l(\mathbf{C})) = \frac{1}{\mathrm{Card}\{S_l(\mathbf{C})\}} \cdot \sqrt{\sum_{P \in S_l(\mathbf{C})} \left(\mathbf{I}(P) - \bar{\mathbf{I}}(S_l(\mathbf{C}))\right)^T \left(\mathbf{I}(P) - \bar{\mathbf{I}}(S_l(\mathbf{C}))\right)}, \tag{2}$$

where $\mathbf{I}(P)$ is the color of the pixel P in the image $\mathbf{I}$, and $\bar{\mathbf{I}}(S_l(\mathbf{C}))$ is the mean color of the pixels which belong to $S_l(\mathbf{C})$:

$$\bar{\mathbf{I}}(S_l(\mathbf{C})) = \frac{1}{\mathrm{Card}\{S_l(\mathbf{C})\}} \cdot \sum_{P \in S_l(\mathbf{C})} \mathbf{I}(P). \tag{3}$$

The local color dispersion measure of the subset $S_l(\mathbf{C})$ is defined as the mean of the color dispersion measures $\sigma(N[S_l(\mathbf{C})](P))$ of the subsets $N[S_l(\mathbf{C})](P)$ of all the pixels P in $S_l(\mathbf{C})$:

$$\sigma_{\mathrm{local}}(S_l(\mathbf{C})) = \frac{1}{\mathrm{Card}\{S_l(\mathbf{C})\}} \cdot \sum_{P \in S_l(\mathbf{C})} \sigma(N[S_l(\mathbf{C})](P)). \tag{4}$$

Note that the above local color dispersion at each pixel in the subset $S_l(\mathbf{C})$ only takes into account the colors of its neighbors that also belong to $S_l(\mathbf{C})$.

The homogeneity degree $HD_l(\mathbf{C})$ is then defined as

$$HD_l(\mathbf{C}) = \begin{cases} \dfrac{\sigma_{\mathrm{local}}(S_l(\mathbf{C}))}{\sigma(S_l(\mathbf{C}))}, & \text{if } \sigma(S_l(\mathbf{C})) \neq 0, \\ 1, & \text{otherwise.} \end{cases} \tag{5}$$

When the color points corresponding to the pixels in the subset $S_l(\mathbf{C})$ give rise to a compact cluster in the color space, the homogeneity degree computed at $\mathbf{C}$ is close to 1. On the opposite, when those color points form several distinct clusters, the homogeneity degree is close to 0.

3.2. Spatial-color compactness function

The spatial-color compactness function (sccf) is a trivariate function whose value at each color point $\mathbf{C}$ is defined as the product of its connectedness and homogeneity degrees:

$$\mathrm{sccf}(\mathbf{C}) = CD_l(\mathbf{C}) \cdot HD_l(\mathbf{C}), \tag{6}$$

where the edge length l of the cube $\mathcal{D}_l$, used to process the degrees all over the color space, is adjusted by the analyst. A high value of sccf($\mathbf{C}$) indicates that the pixels in the subset $S_l(\mathbf{C})$ are highly connected in the image ($CD_l(\mathbf{C})$ close to 1) and that the color points corresponding to these pixels are concentrated in the color space ($HD_l(\mathbf{C})$ close to 1). Conversely, a low value of sccf($\mathbf{C}$) means that the pixels in the subset $S_l(\mathbf{C})$ are scattered in the image ($CD_l(\mathbf{C})$ close to 0) and/or that the color points of these pixels do not form a distinct compact cluster in the color space ($HD_l(\mathbf{C})$ close to 0).

Figure 4(a) shows the sccf of synthetic image in Figure 2(a), computed with the length l set to 7 in order to ensure that the pixel subsets $S_l(\mathbf{C})$ are populated enough. Let us consider three different color points of the color space, respectively, $\mathbf{C_1}$, $\mathbf{C_2}$, and $\mathbf{C_3}$, highlighted as color patches on this figure. We can see that the sccf values are high for both $\mathbf{C_1}$ and $\mathbf{C_3}$ color points, since most of the pixels of the subsets $S_l(\mathbf{C_1})$ and $S_l(\mathbf{C_3})$ are connected to each other in the image, and since their colors are close together (see Figures 4(b) and 4(d)). Note that these two color points are located in the two modes to be detected. On the opposite, at color point $\mathbf{C_2}$ located in the main valley, the sccf value is low since the pixels of the subset $S_l(\mathbf{C_2})$ are scattered in the image (see Figure 4(c)). It is noticeable that the sccf highlights these two modes which were not so obviously distinguishable on the histogram of Figure 2(b).

4. MODE DETECTION BY A FUZZY MORPHOLOGICAL TRANSFORMATION OF THE sccf

4.1. Introduction

Basic binary morphological tools have proved to be suited for object segmentation [24] and for nonglobular mode detection [25]. Park has proposed to detect the modes by applying an adaptive dilation to the closing of the binary 3D histogram, provided by thresholding the difference between two Gaussian smoothed 3D histograms [26]. The aim of this adaptive dilation scheme is to make two adjacent modes meet each other at the valleys of the binary 3D histogram, while preventing the modes to expand towards empty bins. If two adjacent modes meet during dilation, the process is stopped in the direction in which they tend to merge. The process is completed either after a prespecified maximum number of iteration steps or when no mode can be dilated any more. The results depend both on the size of the structuring element used by morphological operators, and on the choice of the color space.

Multivalued morphological operators have also been used to improve mode detection [27, 28]. Shafarenko has proposed to apply the watershed algorithm to the chromaticity 2D histogram coded in the CIE (u^*, v^*) chromatic plane [29]. The acquisition noise is first reduced thanks to a Gaussian filtering. The smoothed histogram is then analyzed by the watershed algorithm in order to detect the modes which correspond to the pixel classes. Xue et al. consider three smoothed 2D histograms which represent the color distribution projected on the (R, G), (R, B), and (G, B) chromatic planes [11]. The watershed algorithm is first applied to each of the three smoothed 2D histograms in order to identify the modes in each chromatic plane, and

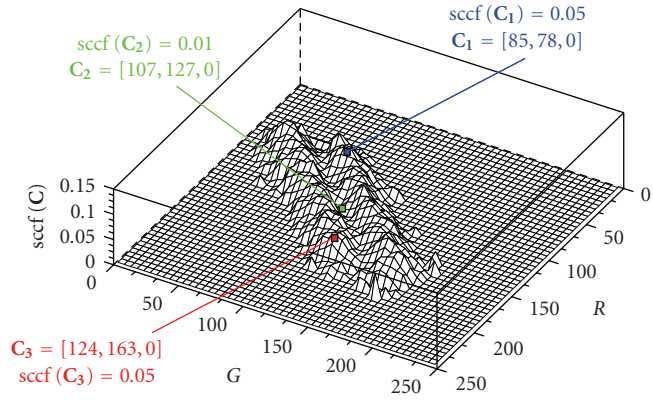

(a) Spatial-color compactness function ($l = 7$)

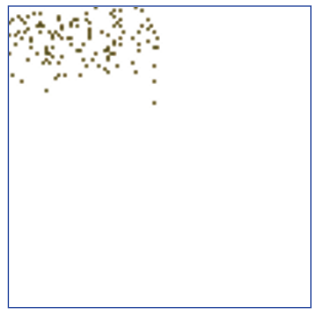

(b) Pixel subset $S_l(\mathbf{C}_1)$

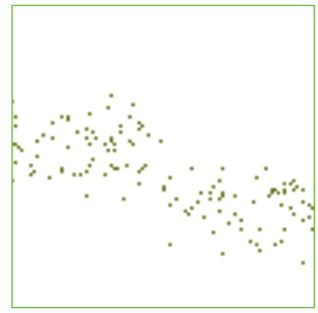

(c) Pixel subset $S_l(\mathbf{C}_2)$

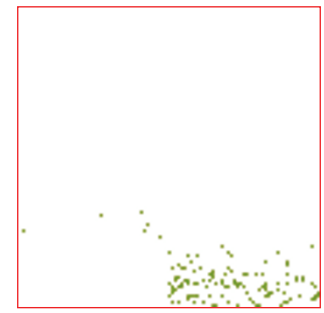

(d) Pixel subset $S_l(\mathbf{C}_3)$

FIGURE 4: Spatial-color compactness function of the synthetic image in Figure 2(a), with three different color points and their corresponding pixel subsets.

then to yield the three different corresponding segmented images. In the last stage, these images are combined by means of a region split and merge process, using the spatial information from the 2D segmentations for the splitting step while taking into account the color coded in the CIE (L^*, a^*, b^*) space during the merging step.

The quality of segmentation results provided by these methods strongly depends on the quality of mode detection. Since only the color distribution is represented by the color histogram, it is challenging to detect the modes which correspond to the actual pixel classes to be retrieved. That is the reason why we choose the sccf as the describing function of the image.

4.2. From the sccf to the fuzzy set "mode"

As described in the previous section, the color points at which the sccf reaches high values are likely to belong to the modes associated with the pixel classes to be constructed. On the opposite, the color points at which the sccf values are low are located in the valleys and do not stand a chance to belong to any mode.

Therefore, we propose to normalize the sccf in order to compute the degree with which each color point $\mathbf{C}$ belongs to a mode. In other words, the normalized sccf evaluates the confidence degree in the statement "$\mathbf{C}$ belongs to a detected mode associated with a pixel class", and can be considered as a *mode membership function* μ_M characterizing the fuzzy set "Mode" denoted M and defined on the color space $\mathcal{C}$:

$$\forall \mathbf{C} \in \mathcal{C}, \quad \mu_M(\mathbf{C}) = \frac{\text{sccf}(\mathbf{C})}{\max_{\mathbf{C}' \in \mathcal{C}} \{\text{sccf}(\mathbf{C}')\}}. \tag{7}$$

High values of μ_M (close to 1) correspond to color points $\mathbf{C}$ belonging to the modes, while low values (close to 0) are associated with color points lying in the valleys between the modes.

As it can be seen on the example of Figure 5, the mode membership function associated with the sccf of Figure 4(a) exhibits many irregularities, which makes the direct detection of the modes a tough task. In order to facilitate this detection, we propose to perform a transformation of the fuzzy set "mode" M, that is, a transformation of the mode membership function μ_M, in order to enhance the modes while enlarging the valleys.

Mathematical morphology is a set theory which provides tools capable of such effects. Indeed, the most basic morphological operators, erosion, and dilation are often combined in pair to result in the opening, wellknown for its filtering properties [30]. The main effect of erosion is to enlarge the valleys by eliminating the irregularities of the distribution, but this operation also tends to shrink the modes. On the other hand, dilation is used to enhance the modes, but it also tends to fill the valleys [8].

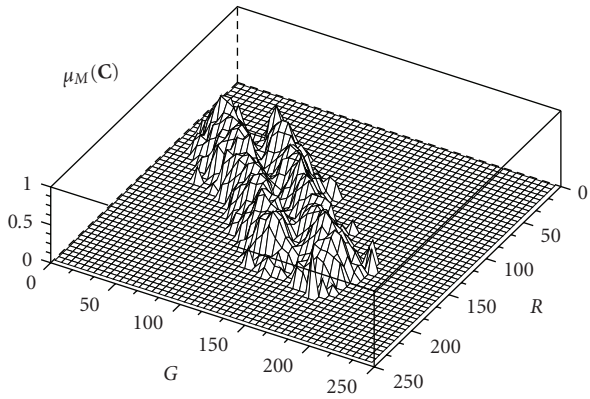

Figure 5: Mode membership function of the synthetic image in Figure 2(a).

We propose to transform the fuzzy set "mode" M, and therefore its associated mode membership function μ_M, by means of fuzzy morphological operators which aim at increasing the contrast between modes and valleys. The key point is to exploit the advantages of these two basic operations of erosion and dilation while avoiding their drawbacks. Such an idea has already been explored in [31], where the mode membership function is extracted thanks to a fuzzification step involving a convexity analysis of the color histogram. However, this method needs the adjustment of many parameters and its success highly depends on the result of the histogram fuzzification step. Moreover, since the membership function introduced in [31] ignores the spatial location of the colors in the image plane, the pixel classes associated with the detected modes may not correspond to the actual regions in the image. So, in this paper, we propose to apply these interesting fuzzy morphological operators to the mode membership function, derived from the sccf, in order to detect the modes.

4.3. Classical fuzzy erosion and dilation operators

The selected classical fuzzy erosion and dilation operators are those which generate the strongest effects of erosion and dilation [32]. They use a fuzzy structuring element defined by its cube $\mathcal{D}_s$ of edge length s and by its membership function γ called the *structuring function*.

In this way, the selected fuzzy erosion E_γ and fuzzy dilation D_γ operators, applied to the mode membership function μ_M at a color point $\mathbf{C}$, are defined in the literature as

$$E_\gamma[\mu_M(\mathbf{C})] = \min_{\mathbf{C}' \in \mathcal{D}_s(\mathbf{C})} \{\max\{\mu_M(\mathbf{C}'), 1 - \gamma(d^\infty(\mathbf{C}, \mathbf{C}'))\}\},$$
$$D_\gamma[\mu_M(\mathbf{C})] = \max_{\mathbf{C}' \in \mathcal{D}_s(\mathbf{C})} \{\min\{\mu_M(\mathbf{C}'), \gamma(d^\infty(\mathbf{C}, \mathbf{C}'))\}\}. \quad (8)$$

The structuring function γ used by the erosion and dilation operators depends on the infinity norm distance $d^\infty(\mathbf{C}, \mathbf{C}') = \max(|C_R - C'_R|, |C_G - C'_G|, |C_B - C'_B|)$ between $\mathbf{C}$ and any of its adjacent color points $\mathbf{C}'$ in $\mathcal{D}_s(\mathbf{C})$.

As an illustration, let us consider the mode membership function μ_M of Figure 5, and the binary structuring function γ defined as

$$\gamma(d^\infty(\mathbf{C}, \mathbf{C}')) = \begin{cases} 1, & \text{if } \mathbf{C}' \in \mathcal{D}_s(\mathbf{C}), \\ 0, & \text{otherwise.} \end{cases} \quad (9)$$

The eroded and dilated membership functions $E_\gamma[\mu_M]$ and $D_\gamma[\mu_M]$ are presented in Figures 6(a) and 6(b), respectively, s being set to the same value as the cube edge length l used to compute the sccf. This example shows that the classical fuzzy erosion tends to enlarge the valleys while shrinking the modes, whereas the classical fuzzy dilation tends to enlarge the modes while filling the valleys.

4.4. Fuzzy erosion and dilation operators specifically designed for mode detection

4.4.1. Fuzzy operators

In order to facilitate the detection of the modes, it would be pertinent to define a fuzzy erosion operator which enlarges the valleys without shrinking the modes, and a fuzzy dilation operator which enhances the modes without filling the valleys. To be more specific, if a color point $\mathbf{C}$ is close to a mode, it is relevant to strengthen the dilation effect at the location of this color point $\mathbf{C}$ and to limit the erosion effect in order to preserve that mode. Moreover, this color point more likely belongs to this mode when its adjacent color points $\mathbf{C}'$ are also close to the same mode. Conversely, if the color point $\mathbf{C}$ is far from all modes, it is probably located in a valley. In this case, it is useful to erode the mode membership function at the location of this color point without dilating it. Such a color point is all the more likely located within a valley than its adjacent color points are also located within a valley. This implies to erode or dilate the mode membership function more or less, depending on the location of each color point in the color space and on its adjacent color points.

In the classical definitions of the fuzzy operators described by (8), the structuring function γ depends on the infinity norm distance between the considered color point $\mathbf{C}$ and each of its adjacent color points $\mathbf{C}'$, but does not depend on their mode membership degrees. However, if the mode membership degree of an adjacent color point is high, it would be interesting to take it into account only for the dilation, but not for the erosion. On the other hand, if the membership degree of an adjacent color point is low, its contribution should be stronger for the erosion than for the dilation. This means that both the fuzzy erosion and dilation operators should be defined by their own specific structuring functions:

$$E'_{\gamma_E}[\mu_M(\mathbf{C})] = \min_{\mathbf{C}' \in \mathcal{D}_s(\mathbf{C})} \{\max\{\mu_M(\mathbf{C}'), 1 - \gamma_E(\mathbf{C}')\}\}, \quad (10)$$

$$D'_{\gamma_D}[\mu_M(\mathbf{C})] = \max_{\mathbf{C}' \in \mathcal{D}_s(\mathbf{C})} \{\min\{\mu_M(\mathbf{C}'), \gamma_D(\mathbf{C}')\}\}, \quad (11)$$

with γ_E and γ_D being described in Sections 4.4.2 and 4.4.3, respectively.

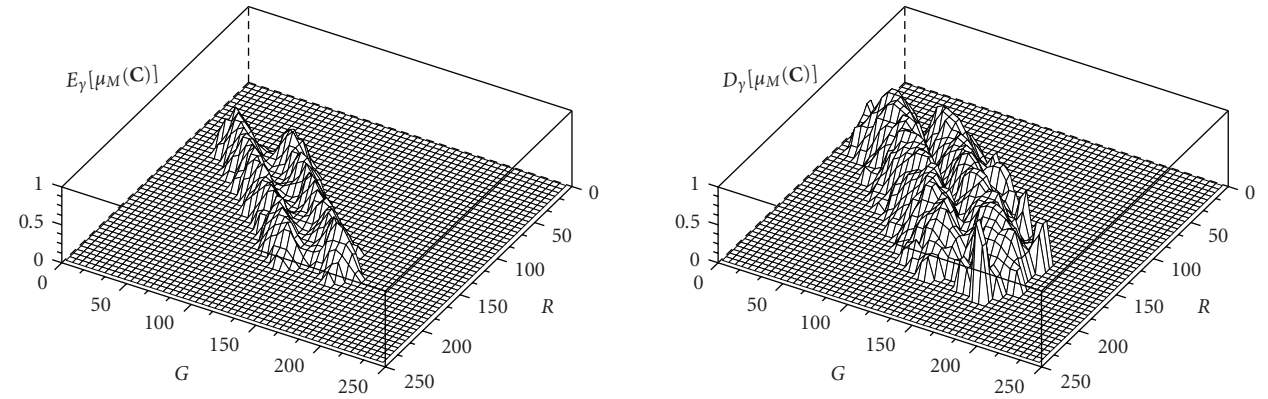

(a) Classical fuzzy erosion

(b) Classical fuzzy dilation

Figure 6: Results of the classical fuzzy morphological operations applied to the mode membership function of Figure 5 ($s = 7$).

4.4.2. Specific structuring function associated with the fuzzy erosion

The fuzzy erosion, expressed by (10), is performed using a specific structuring function γ_E defined for each of the adjacent color points $\mathbf{C}'$ in the structuring element cube $\mathcal{D}_s(\mathbf{C})$. We propose to define this structuring function γ_E as

$$\gamma_E(\mathbf{C}') = \begin{cases} 1, & \text{if } f_M(\mathbf{C}') \le \overline{f}_M, \\ \mu_M(\mathbf{C}), & \text{otherwise,} \end{cases} \tag{12}$$

where f_M is a decision function and $\overline{f}_M$ the mean value of this function (see (13), (14), and (15)).

The decision function f_M is defined according to the following assumption: in the color space, an adjacent color point $\mathbf{C}'$ (included in the cube $\mathcal{D}_s(\mathbf{C})$) can be located in a mode, in a valley, or in the border between the two. An adjacent color point $\mathbf{C}'$, which is close to the border between a valley and a mode, is characterized by significant local variations between its mode membership degree and the mode membership degrees of its adjacent color points. The combination of these two criteria is well suited to decide if a color point is located in a mode, in a valley, or at a border. So, the decision function f_M is defined at each adjacent color point $\mathbf{C}'$ as

$$f_M(\mathbf{C}') = \mu_M(\mathbf{C}') \cdot (1 - g_{\mu_M}(\mathbf{C}')). \tag{13}$$

In this equation, g_{μ_M} is an approximation of the morphological gradient of μ_M evaluated by the difference between the crisp dilation and the crisp erosion of the mode membership function computed at the color point $\mathbf{C}'$ [8]:

$$g_{\mu_M}(\mathbf{C}') = \max_{\mathbf{C}'' \in \mathcal{D}_w(\mathbf{C}')} \{\mu_M(\mathbf{C}'')\} - \min_{\mathbf{C}'' \in \mathcal{D}_w(\mathbf{C}')} \{\mu_M(\mathbf{C}'')\}, \tag{14}$$

where the edge length w of the cube $\mathcal{D}_w$ used to process this morphological gradient is adjusted by the analyst. Empirically, we set this edge length to $w = 2s - 1$.

The mean value $\overline{f}_M$ of the decision function f_M is defined as

$$\overline{f}_M = \overline{\mu}_M \cdot (1 - \overline{g}_{\mu_M}), \tag{15}$$

where $\overline{\mu}_M$ is the mean mode membership degree of the color points where the mode membership degree is nonzero. In the same way, $\overline{g}_{\mu_M}$ is the mean of the nonzero responses of the morphological gradient of μ_M in the color space.

In (12), if the decision function value $f_M(\mathbf{C}')$ at an adjacent color point $\mathbf{C}'$ is lower than or equal to the mean value $\overline{f}_M$, $\mathbf{C}'$ is considered as being located within a valley or at a border close to a valley. In this case, $\gamma_E(\mathbf{C}')$ used by (10) is set to 1, so that $\mathbf{C}'$ strongly contributes to the fuzzy erosion operation at the color point $\mathbf{C}$. Conversely, if $f_M(\mathbf{C}')$ is higher than $\overline{f}_M$, $\mathbf{C}'$ is considered as being located in a mode or at a border close to a mode. In this case, $\gamma_E(\mathbf{C}')$ is set to $\mu_M(\mathbf{C})$, so that the contribution of this adjacent color point $\mathbf{C}'$ to the fuzzy erosion operation at the color point $\mathbf{C}$ is very weak. Thus, this fuzzy erosion using the structuring function γ_E tends to deepen the valleys without shrinking the modes.

4.4.3. Specific structuring function associated with the fuzzy dilation

According to the same idea, the structuring function γ_D associated with the fuzzy dilation expressed by (11) can be defined as

$$\gamma_D(\mathbf{C}') = \begin{cases} 1, & \text{if } f_M(\mathbf{C}') > \overline{f}_M, \\ \mu_M(\mathbf{C}), & \text{otherwise.} \end{cases} \tag{16}$$

If the decision function value $f_M(\mathbf{C}')$ is higher than the mean value $\overline{f}_M$, the adjacent color point $\mathbf{C}'$ can be considered as being located within a mode or at a border close to a mode. Its contribution to the fuzzy dilation at the color point $\mathbf{C}$ is then the strongest one. Conversely, if $f_M(\mathbf{C}')$ is lower than $\overline{f}_M$, $\mathbf{C}'$ is considered as being located in a valley or at a border close to a valley, and its influence on the

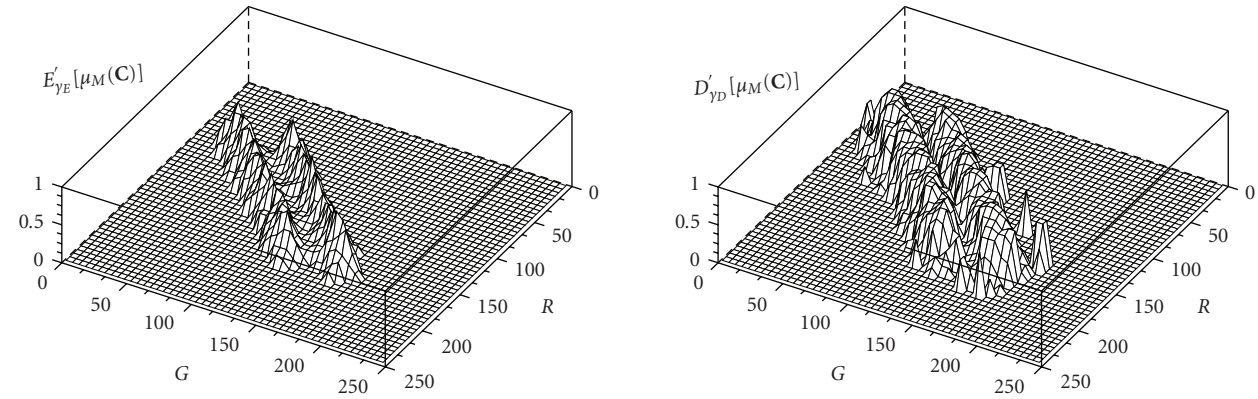

(a) Specific fuzzy erosion (b) Specific fuzzy dilation

FIGURE 7: Results of the fuzzy morphological operations specifically designed for mode detection applied to the mode membership function of Figure 5 ($s = 7, w = 13$).

fuzzy dilation is very weak. Thus, dilating the membership function μ_M using this structuring function γ_D tends to enhance the modes without filling the valleys.

4.4.4. Illustrative results

Figures 7(a) and 7(b), respectively, display the results of the so defined fuzzy erosion and dilation operators applied to the mode membership function of Figure 5, when the edge length s of the structuring element cube is set to $s = 7$, and when the edge length w of the cube used by the morphological gradient is set to $w = 2s - 1 = 13$. Figure 7(a) shows that the mode membership function is only eroded at the color points located in valleys. Moreover, Figure 7(b) shows that μ_M is dilated only at the color points located near the modes.

The results of these specific fuzzy operators can be compared with those obtained by the classical fuzzy morphological operators displayed in Figure 6. For comparison sake, the diagonal ($R + G = 255$) cross-section (see Figure 8(a)) of the mode membership function μ_M is displayed in Figure 8(b) and the results of the application of the different fuzzy operations on this cross-section are presented in Figures 8(c)–8(f). As expected, the classical fuzzy erosion tends to shrink the modes (see Figure 8(c)), while the proposed fuzzy erosion illustrated in Figure 8(d) only tends to deepen the valleys. Furthermore, the classical fuzzy dilation tends to fill the valleys as illustrated in Figure 8(e), while the proposed fuzzy dilation only tends to enhance the modes (see Figure 8(f)). This example shows the improvement in mode enhancement achieved by the proposed fuzzy morphological operators, in comparison with the classical ones.

4.5. Fuzzy morphological transformation for mode detection

In order to take advantage of the two fuzzy operators defined above, we propose to combine them into a fuzzy morphological transformation, which performs a fuzzy erosion of the mode membership function μ_M using the structuring function γ_E, followed by a fuzzy dilation of the resulting mode membership function using the structuring function γ_D.

This transformation, denoted as t, is defined as

$$t[\mu_M] = D'_{\gamma D}[E'_{\gamma E}(\mu_M)]. \tag{17}$$

Figure 9(b) presents the transformed mode membership function $t[\mu_M]$, whose cross-section plot is detailed in Figure 9(d). As required, the modes are enhanced while the main valley is not filled but enlarged. This result can be compared with that of the classical fuzzy opening of μ_M (see Figure 9(a)), whose cross-section plot is detailed in Figure 9(c). So, this figure shows that our transformation outperforms the classical fuzzy opening for mode enhancement.

However, since the effect of this transformation t, yielding the transformed mode membership function denoted by $\widetilde{\mu}_M$, is still rather weak, we propose to iterate it as follows:

$$\begin{aligned} &\widetilde{\mu}_M^0 = \mu_M, \\ &\widetilde{\mu}_M^n = t[\widetilde{\mu}_M^{n-1}], \quad n = 1, 2, 3, \ldots, \end{aligned} \tag{18}$$

until the resulting mode membership function becomes stable. The global fuzzy transformation, denoted by T, yields the stable function $\widetilde{\mu}_M^\infty$.

Figure 10(a) shows the transformed membership function $\widetilde{\mu}_M^2$ obtained after 2 iteration steps, while Figure 10(b) shows the stable mode membership function $\widetilde{\mu}_M^\infty$, reached after 15 iteration steps. We can see on the latter figure that the two modes are well enhanced. It is also important to notice that the highest and lowest mode membership degrees, respectively associated with the modes and the valleys, are preserved. Indeed, when performed at a color point corresponding to a local maximum of the mode membership function, the fuzzy dilation propagates this high degree to the adjacent color points which are considered as being located in this mode or at a border. Conversely,

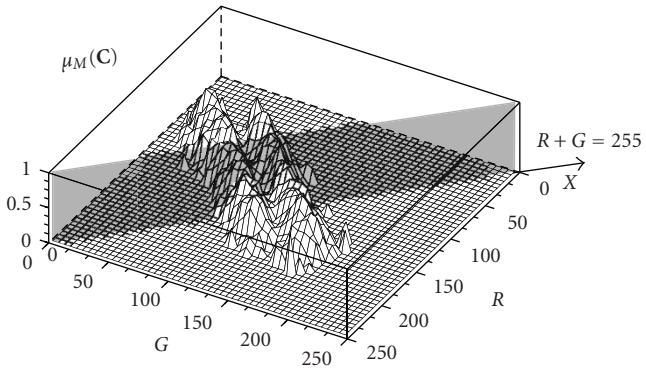

(a) Original mode membership function μ_M and cross-section

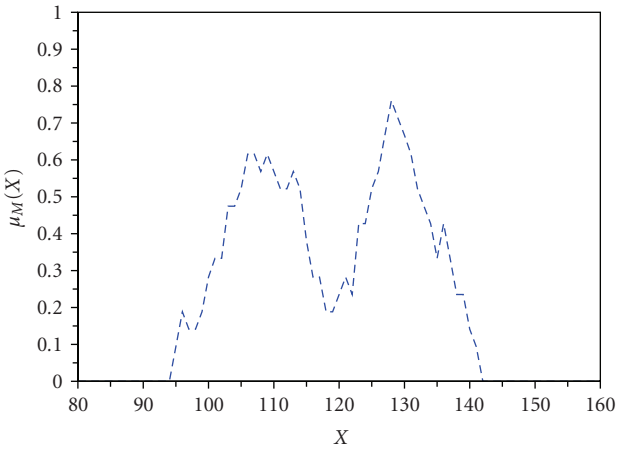

(b) Mode membership function μ_M

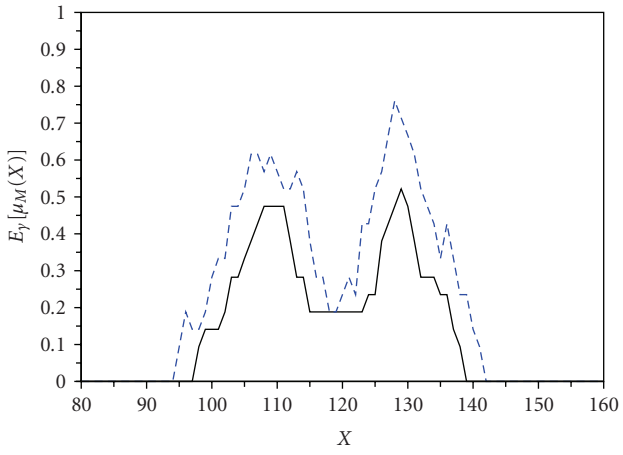

(c) Classical fuzzy erosion E_γ of μ_M

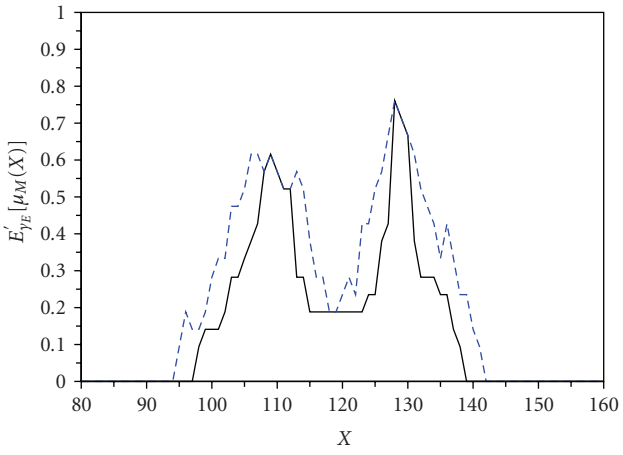

(d) Classical fuzzy erosion E'_γ of μ_M

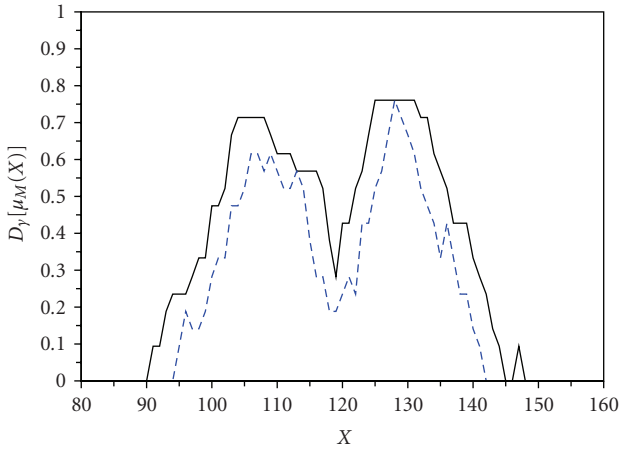

(e) Classical fuzzy dilation D_γ of μ_M

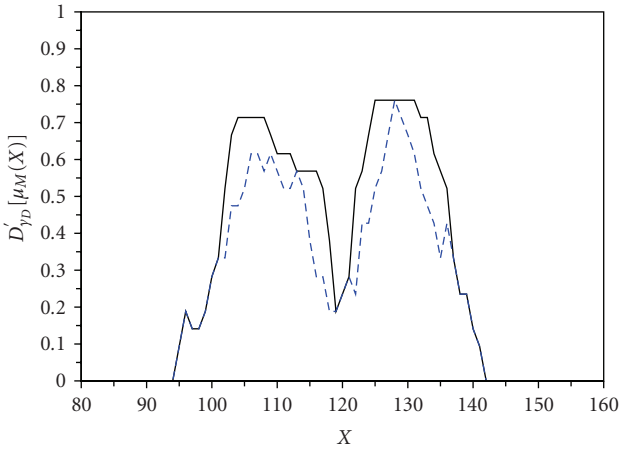

(f) Specific fuzzy dilation $D'_{\gamma D}$ of μ_M

FIGURE 8: Comparison on cross-sections between the classical fuzzy operators and those specific to mode detection. The original mode membership function μ_M is plotted as dashed lines.

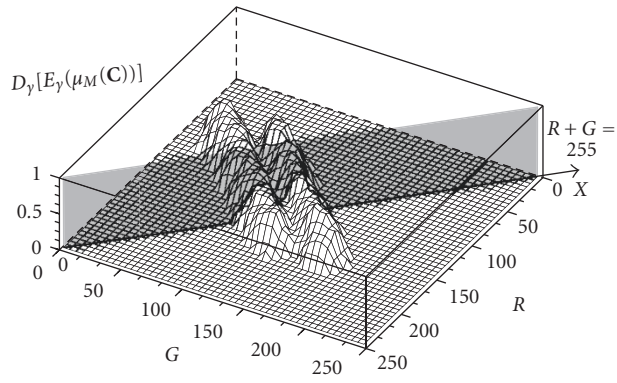

(a) Classical fuzzy opening $D_\gamma[E_\gamma]$ of μ_M and cross-section

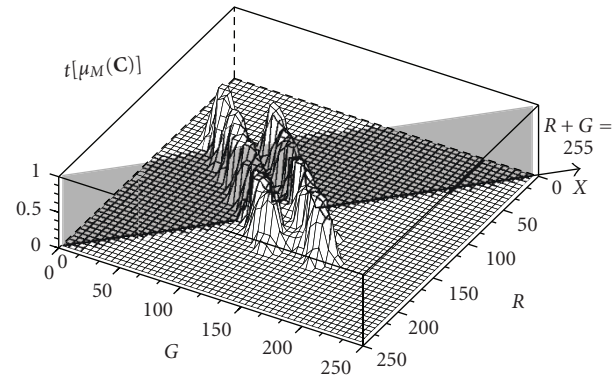

(b) Specific transformation t of μ_M and cross-section

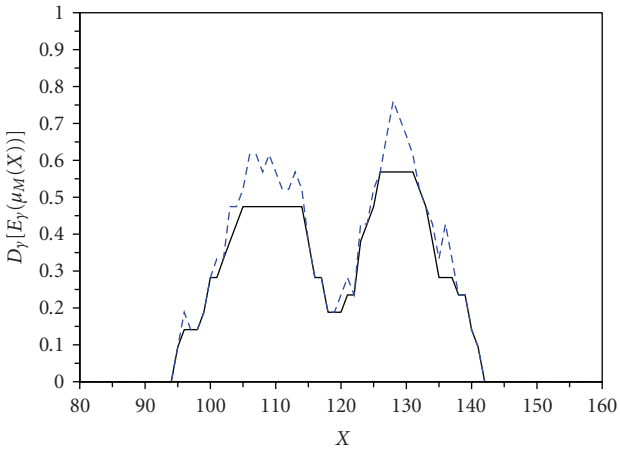

(c) Cross-section plot of the classical fuzzy opening $D_\gamma[E_\gamma]$ of μ_M

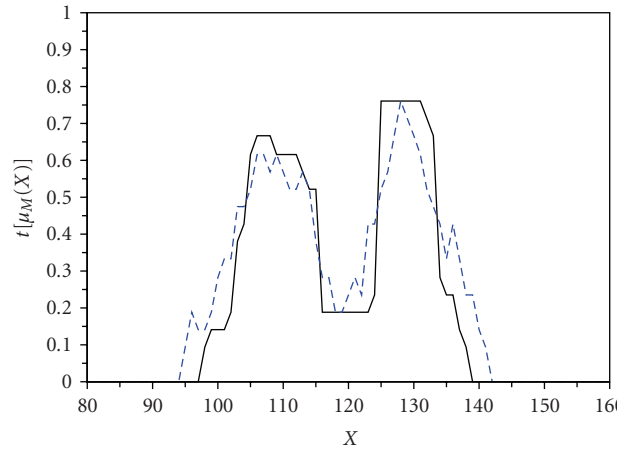

(d) Cross-section plot of the specific transformation t of μ_M

FIGURE 9: Comparison on cross-sections between the classical fuzzy opening and the fuzzy transformation t. The original mode membership function μ_M is plotted as dashed lines.

when performed at a color point corresponding to a local minimum of the mode membership function, the proposed erosion propagates this low degree to the adjacent color points which are considered as being located in this valley or at a border.

Finally, the modes are easily detected thanks to the defuzzification of the transformed mode membership function $\widetilde{\mu}_M^\infty$ which simply consists in thresholding $\widetilde{\mu}_M^\infty$. More precisely, at any color point $\mathbf{C}$, if $\widetilde{\mu}_M^\infty(\mathbf{C})$ is greater than $\overline{\mu}_M$ already defined in Section 4.4.2, this color point is then considered as belonging to a mode of the color space.

5. EXPERIMENTAL RESULTS

In order to illustrate the behavior and efficiency of our method, hereafter called *sccf mode detection*, in case of spatially nonuniform lighting, we propose to apply it first to synthetic images. Then, we consider benchmark natural images extracted from Berkeley database (cf. http://www.eecs.berkeley.edu/Research/Projects/CS/vision/grouping/segbench/) [33], and compare automatic segmentation results with human segmentation ones.

5.1. Synthetic images

The sccf mode detection scheme is first applied to the synthetic image in Figure 2(a) already used to illustrate our work. Figure 10(b) shows the resulting transformed mode membership function $\widetilde{\mu}_M^\infty$, in which the two modes are very well enhanced with respect to their initial shapes. After they have been detected by the defuzzification stage, these two modes are identified by a simple connected component analysis procedure achieved in the color space (see Figure 11(a)).

As each identified mode corresponds to a pixel class, all the pixels whose colors are located in an identified mode define the prototypes of the corresponding class. Figure 11(b) shows the prototypes of the two pixel classes labeled as false colors, white-marked pixels being not yet assigned to any class. This image shows that only a few prototype pixels are misclassified. It illustrates that the constructed classes well correspond to the two regions to be retrieved.

The next classification procedure stage consists in labeling all the pixels which are not yet assigned, thanks to the belief-based pixel labeling procedure proposed by

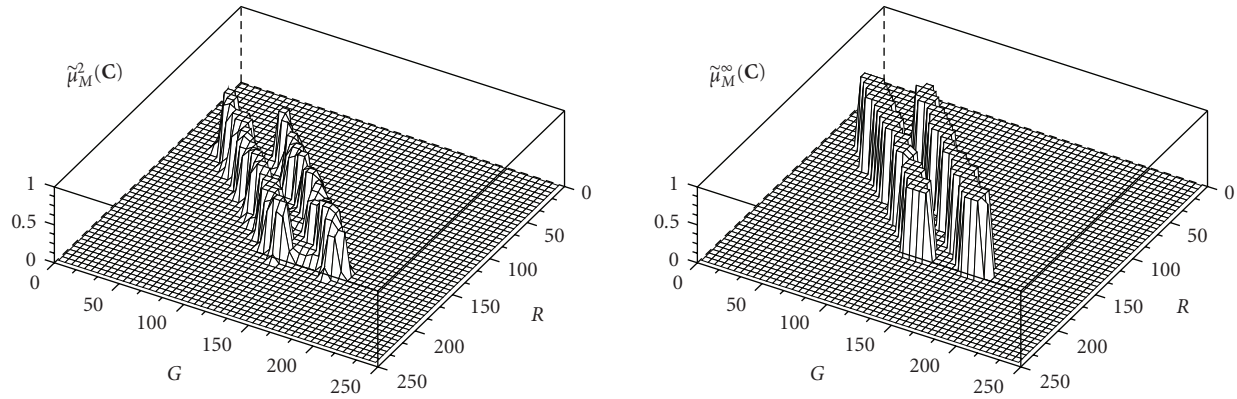

(a) Transformation of μ_M after 2 iteration steps

(b) Final mode membership function $\widetilde{\mu}_M^\infty = T(\mu_M)$

FIGURE 10: Results of the fuzzy morphological transformations specifically designed for mode detection applied to the mode membership function of Figure 5 ($s = 7, w = 13$).

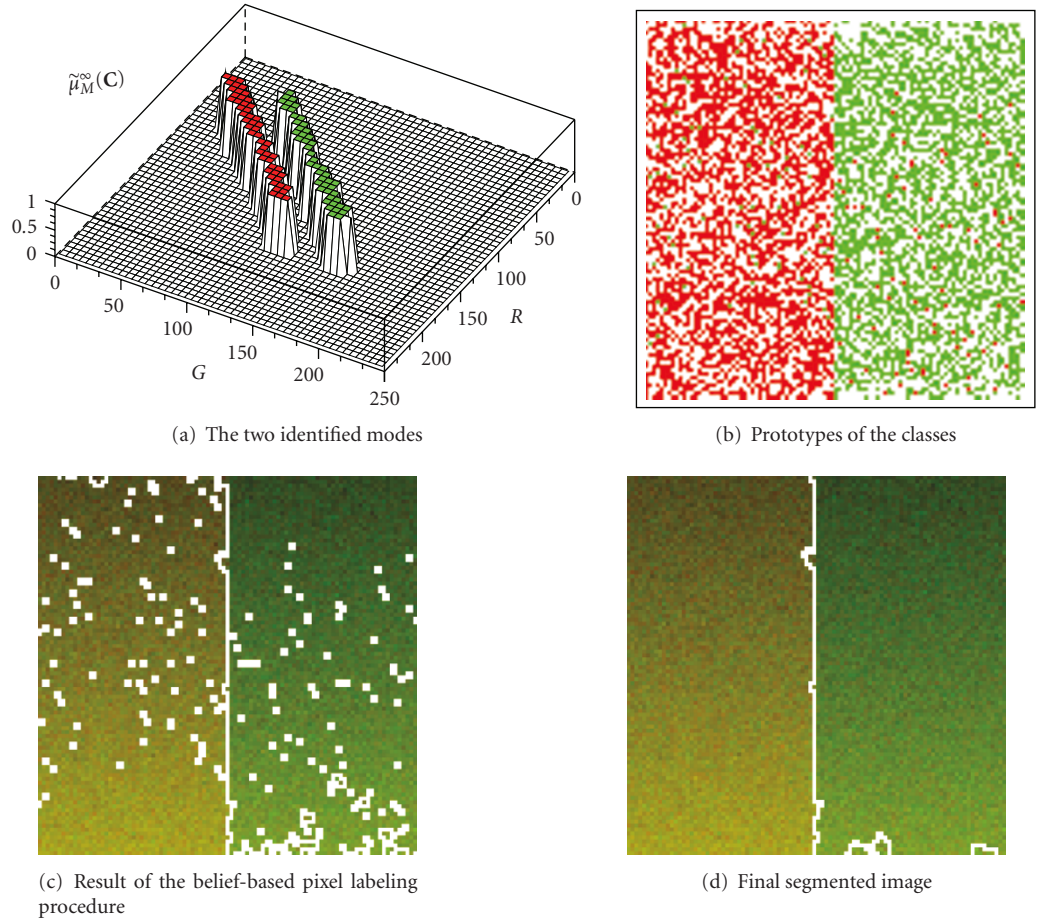

(a) The two identified modes

(b) Prototypes of the classes

(c) Result of the belief-based pixel labeling procedure

(d) Final segmented image

FIGURE 11: Segmentation of the synthetic image in Figure 2(a) by the sccf mode detection scheme.

Vannoorenberghe [34]. In the resulting segmented image in Figure 11(c), the connected pixels assigned to the same classes form regions whose edges are white marked. This image shows that the two original regions of Figure 2(a) are well reconstructed. The small regions caused by misclassified pixels are easily erased by a postprocessing stage based on the region surface size. Thus, all the pixels belonging to a region whose size is lower than 20 pixels are first reset to the unassigned state, and the belief-based pixel labeling procedure is then reperformed. The final segmentation result provided by this postprocessing stage is presented in Figure 11(d). The comparison of this segmentation result with those provided

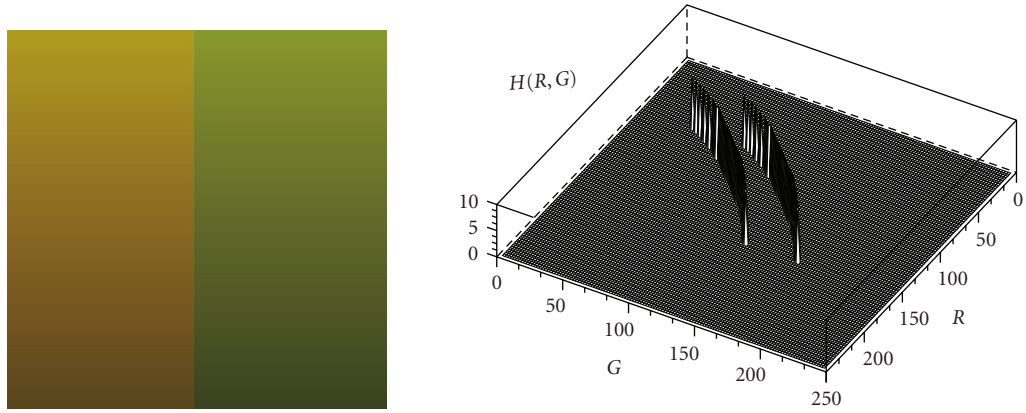

(a) Synthetic image (b) Histogram in the (R, G) plane

FIGURE 12: A synthetic image with nonlinear color distribution.

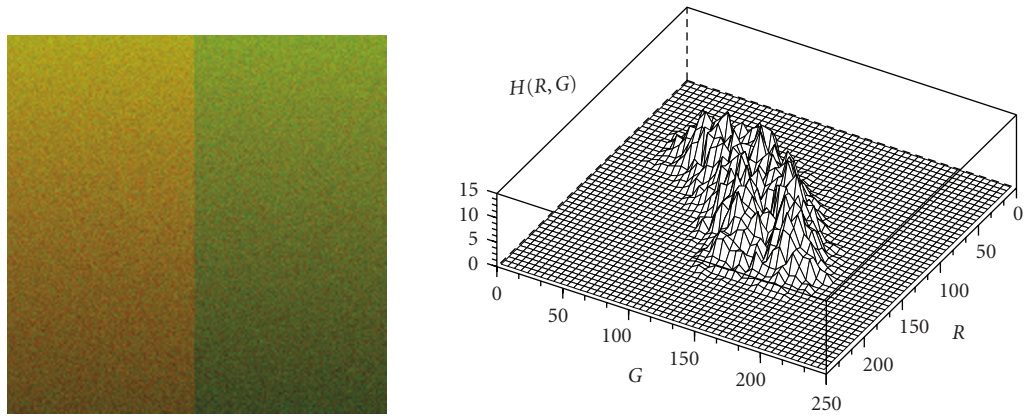

(a) Noisy synthetic image (b) Histogram in the (R, G) plane

FIGURE 13: A synthetic image, corrupted by acquisition noise, with nonlinear color distribution.

by the tested classical methods presented in Figure 3 shows the improvement of our approach in detecting nonglobular modes corresponding to regions whose color distributions strongly overlap.

In the previous illustrative example of Figure 2(a), the (R, G) color component variation is too coarse to realistically represent a spatially nonuniform lighting. This variation should not follow a line in the (R, G) chromatic plane, but rather an arc of ellipse. Let us consider the synthetic image in Figure 12(a), where the (R, G) color components change along elliptic arcs with respect to the pixel row coordinates, as shown by the histogram presented in Figure 12(b). Like the first synthetic image in Figure 1(a), this image has been corrupted by a noncorrelated Gaussian noise, with a standard deviation equal to 10 (see Figure 13(a)). The histogram of this image (see Figure 13(b)) shows that, since the color distributions of the two regions to be retrieved strongly overlap and since the valley between the two modes is not linear, the two modes are hardly detectable by an automatic processing of this histogram.

Figure 14(a) shows the mode membership function μ_M associated with the sccf describing this image, processed with $l = 7$. The two modes identified by the sccf mode detection procedure applied to this mode membership function are displayed in Figure 14(b). Most of the prototype pixels presented in Figure 14(c) are well classified, and the final segmented image in Figure 14(d) shows that the two regions are well reconstructed. This result can be compared with those obtained by the JSEG, mean shift, and SCDA algorithms presented in Figure 15. The comparison of these images shows that the sccf mode detection technique outperforms these classical spatial-color pixel classification methods when the modes are nonglobular in the color space.

In case of a synthetic image, the result of the automatic classification procedure can be compared with the ground truth by computing the error rate. This error rate is defined as the ratio of the number of misclassified pixels to the size of the considered image. Table 1 displays the classification error rates obtained by the four tested approaches applied to the synthetic images in Figures 2(a) and 13(a). This table

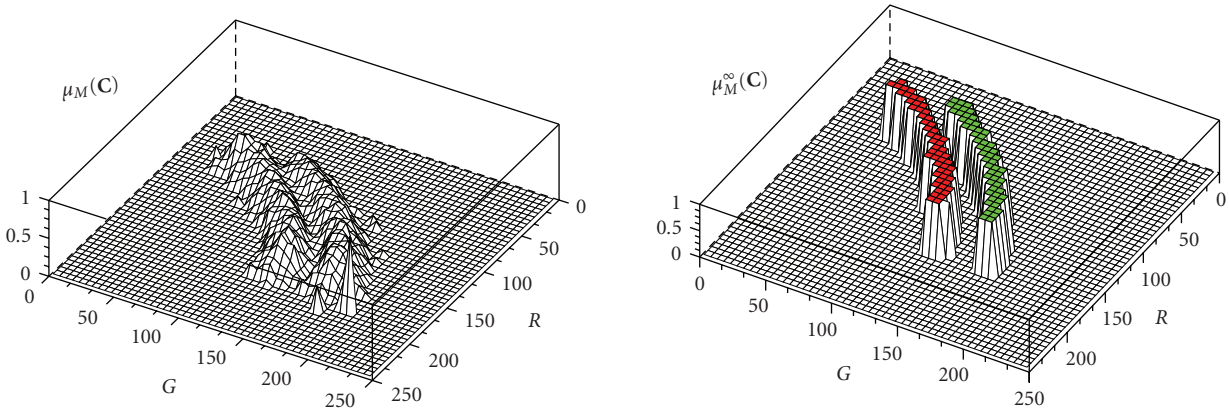

(a) Mode membership function

(b) The two identified modes

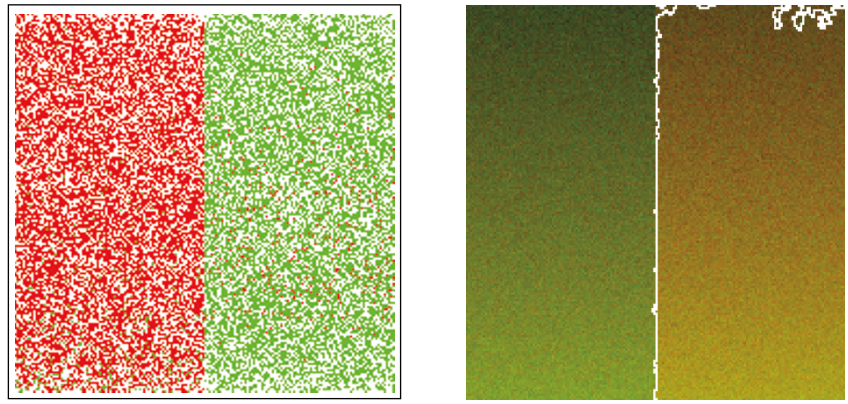

(c) Prototypes of the classes

(d) Final segmented image

Figure 14: Segmentation of the synthetic image in Figure 13(a) by the sccf mode detection scheme.

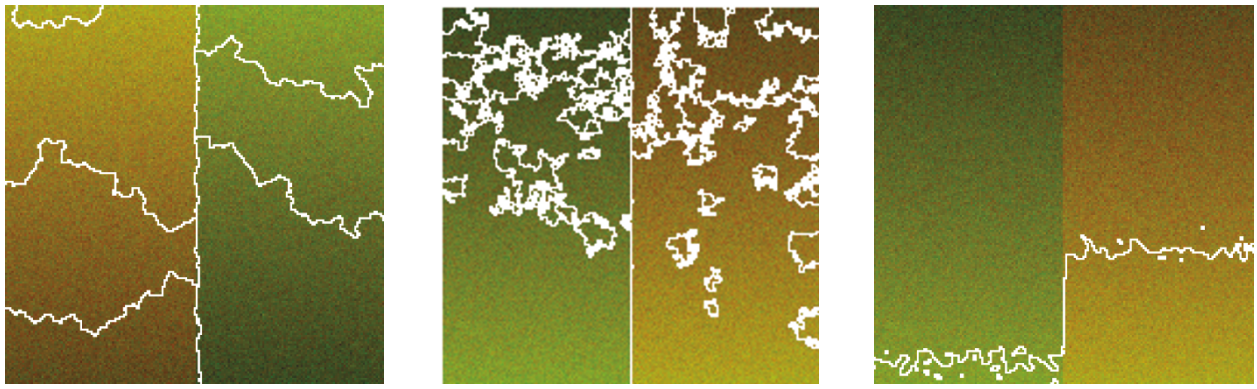

(a) JSEG [16]

(b) Mean shift [20]

(c) SCDA [21]

Figure 15: Segmentation results of the synthetic image in Figure 13(a) provided by well-known spatial-color image segmentation methods.

Table 1: Classification error rates on two synthetic images.

Image	Synthetic image (Figure 2(a))	Noisy synthetic image (Figure 13(a))
JSEG [16]	53%	52%
Mean shift [20]	30%	35%
SCDA [21]	37%	37%
sccf mode detection	3%	3%

(a) Human segmentation

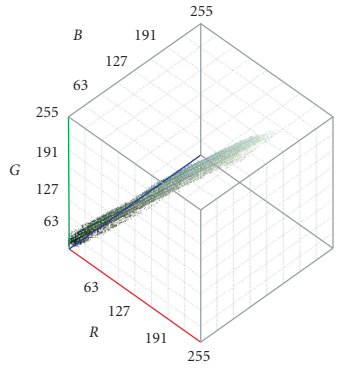

(b) Color distribution

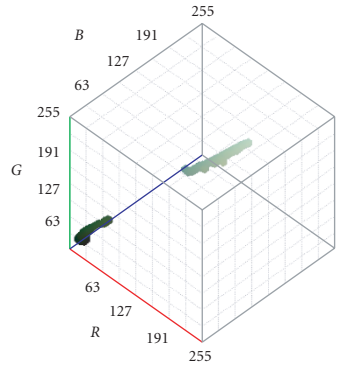

(c) 3 detected modes ($l = 7$)

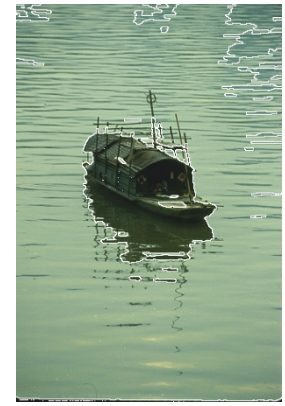

(d) Segmentation by sccf mode detection ($l = 7$)

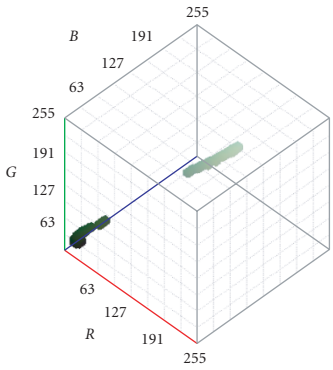

(e) 2 detected modes ($l = 9$)

(f) Segmentation by sccf mode detection ($l = 9$)

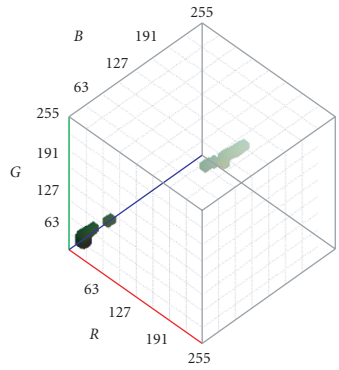

(g) 3 detected modes ($l = 11$)

(h) Segmentation by sccf mode detection ($l = 11$)

(i) JSEG [16]

(j) Mean shift [20]

FIGURE 16: Segmentation results of the *Boat* image.

TABLE 2: Quantitative similarity measures, using the Jaccard index, of segmentation results achieved by different techniques applied to three benchmark natural images.

Image	*Boat* (Figure 16(a))	*Birds* (Figure 17(a))	*Plane* (Figure 18(a))
JSEG [16]	0.10	0.48	0.26
Mean shift [20]	0.02	0.16	0.06
sccf mode detection	0.14	0.48	0.20

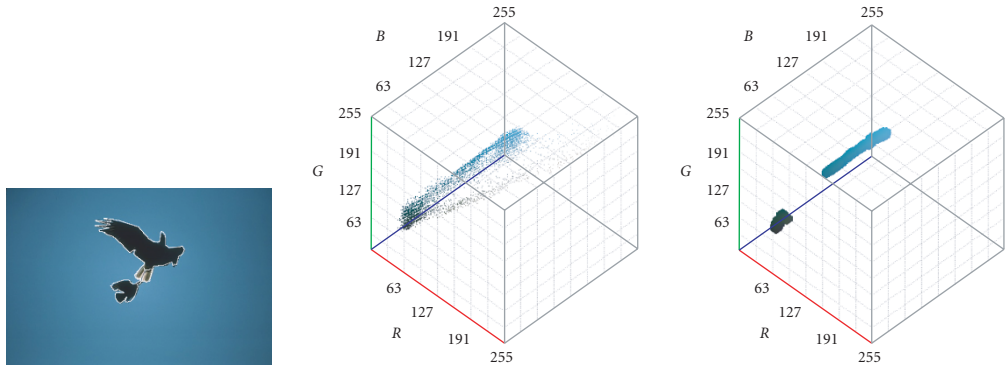

(a) Human segmentation (b) Color distribution (c) 2 detected modes ($l = 9$)

(d) Segmentation by sccf mode detection ($l = 9$) (e) JSEG [16] (f) Mean shift [20]

Figure 17: Segmentation results of the *Birds* image.

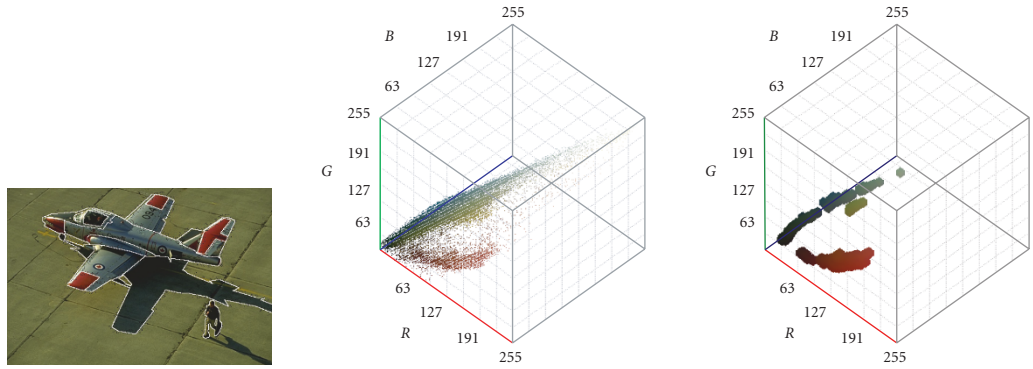

(a) Human segmentation (b) Color distribution (c) 6 detected modes ($l = 9$)

(d) Segmentation by sccf mode detection ($l = 9$) (e) JSEG [16] (f) Mean shift [20]

Figure 18: Segmentation results of the *Plane* image.

shows that the classification error rates obtained by the sccf mode detection technique are significantly lower than those provided by the tested classical approaches.

Our segmentation scheme, implemented on a PC with a Pentium IV 2 GHz microprocessor, requires a processing time of about 60 seconds to segment an image of size 1000×100 pixels. This processing time strongly depends on the size N_{pix} of the image, on the number L of levels used to quantize the color components, and on the cube edge length parameters s and w. Note that the processing time of the sccf

mode detection scheme is mainly due to unoptimized code so far. This time is higher than those of JSEG, mean shift, and SCDA techniques, which are respectively 8 s, 5 s, and 30 s.

To estimate the complexity order of the sccf mode detection approach, we divide it into three successive stages. The first one processes the sccf at the L^3 color points by examining the neighborhood of the N_{pix} pixels. Its complexity order is therefore equal to $N_{\text{pix}} \cdot L^3$. The second stage iteratively applies the morphological transformation t to the mode membership function. The complexity order of the transformation t is equal to $L^3 \cdot (s^3 + w^3)$, since this operation examines the cubes centered at each color point of the color space. Assuming that this transformation is iterated U times until the resulting mode membership function is stable, the complexity order of this second stage is equal to $U \cdot L^3 \cdot (s^3 + w^3)$. The complexity order of the third stage, which assigns the N_{pix} pixels to the constructed classes, is equal to $V \cdot N_{\text{pix}}$, since the belief-based labeling procedure is iterated V times. The complexity order of our segmentation scheme is therefore globally estimated as $L^3 \cdot (N_{\text{pix}} + U \cdot (s^3 + w^3)) + V \cdot N_{\text{pix}}$.

5.2. Benchmark images

In order to show the practical interest of the sccf mode detection procedure, we propose to segment three benchmark natural images (#15088, #135069, and #37073) extracted from Berkeley database [33], respectively, presented in Figures 16(a), 17(a), and 18(a), and hereafter referred to as *Boat*, *Birds*, and *Plane* images. Each of these images shows one human segmentation among the five ones available in Berkeley database, with the edges of the regions being white marked. These three images are retained since the illuminating conditions spatially vary. Moreover, since they contain a few objects to be detected without any ambiguity, the five human segmentations are consistent.

The *Boat* image (see Figure 16(a)) contains one boat above the water. Segmenting it is very difficult since the colors of the pixels representing the water spatially vary. This phenomenon is caused by the nonuniform reflectance properties of the surface of the water illuminated by the sun. The human segmentation regroups the pixels into two main classes associated with the boat and the water. The mode detection is challenging since the color points of this image give rise to one main elongated cluster along the gray axis of the (R, G, B) color space (see Figure 16(b)).

In order to provide some insight into the behavior of the sccf mode detection procedure, we propose to process the sccf with the edge length l ranging from 7 to 11. As previously, we set to l the edge length s of the structuring element cube, and to $2s - 1$ the edge length of w the cube used by the morphological gradient.

Figure 16(d) shows that the sccf mode detection scheme divides the water pixels into two different classes, and regroups the boat pixels into one single class when the length l is set to 7. Figure 16(e) shows that our approach succeeds in detecting the two main modes when l is set to 9. When l is set to 11, the mode which represents the colors of the boat is split into two modes standing for both the boat and its shadow on the water (see Figure 16(g)). However, the segmented images in Figures 16(d), 16(f), and 16(h) show that the sccf mode detection scheme provides relevant segmentations when the illuminating conditions spatially vary all over the image. These segmented images can be compared with those obtained by the JSEG and mean shift techniques, both performed with the default parameter values suggested by the authors (see Figures 16(i) and 16(j)). The sccf mode detection procedure succeeds in providing relevant segmentations of the water area, where the tested classical methods provide oversegmentation. This experiment leads us to set the parameter l to 9 in order to segment the natural images. Note that we do not perform the SCDA method on any of the benchmark images because this last technique needs prior knowledge of the number of classes to be constructed.

The *Birds* image (see Figure 17(a)) contains two birds flying in a blue sky. The intensities of the pixels representing the sky are not uniform all over the image. The human segmentation regroups the pixels into two main classes, which are associated with the birds and the sky. The color points of this image give rise to thin clusters along the gray axis of the (R, G, B) color space (see Figure 17(b)). Figure 17(c) shows that the sccf mode detection procedure succeeds in detecting the two main modes despite the nonequiprobability of the pixel classes. The segmented image in Figure 17(d) points out that the segmentation provided by our scheme is quite close to that of the human segmented imagein Figure 17(a), as are those provided by the JSEG and mean shift methods (see Figures 17(e) and 17(f)).

The *Plane* image (see Figure 18(a)) contains five main pixel classes which correspond to the background, the shadow of the plane, the man, the gray parts, and the red patterns of the plane. Segmenting this image is challenging because of the presence of shadows and highlight effects, and also because the color points give rise to a lot of sparse clusters in the color space (see Figure 18(b)). The segmented image in Figure 18(d) is derived from the modes detected by the sccf mode detection scheme (see Figure 18(c)). We can see that our procedure succeeds in not detecting the thin lines in the background since their surfaces are too small to be represented by the sccf. The segmentation provided by our scheme is consistent with the human one and with that provided by JSEG (see Figure 18(e)). Note that the mean shift technique globally provides oversegmentation (see Figure 18(f)).

In order to provide some quantitative segmentation evaluation, the Jaccard index is used as in [35] to measure the region coincidence between the results of each human segmentation $\mathbf{S}^{\mathcal{H}}$(composed $n^{\mathcal{H}}$ of regions $\mathbf{R}_i^{\mathcal{H}}$, $i = 1, 2, \ldots, n^{\mathcal{H}}$) and each automatic segmentation $\mathbf{S}^{\mathcal{A}}$ (composed of $n^{\mathcal{A}}$ regions $\mathbf{R}_j^{\mathcal{A}}$, $i = 1, 2, \ldots, n^{\mathcal{A}}$), with the human one being considered as the ground truth. For two regions $\mathbf{R}_i^{\mathcal{H}}$ and $\mathbf{R}_j^{\mathcal{A}}$, the Jaccard index is defined as

$$J(\mathbf{R}_i^{\mathcal{H}}, \mathbf{R}_j^{\mathcal{A}}) = \frac{\text{Card}\{\mathbf{R}_i^{\mathcal{H}} \cap \mathbf{R}_j^{\mathcal{A}}\}}{\text{Card}\{\mathbf{R}_i^{\mathcal{H}} \cup \mathbf{R}_j^{\mathcal{A}}\}}. \tag{19}$$

The numerator in (19) measures to which extent the region $\mathbf{R}_j^{\mathcal{A}}$ derived from the automatic segmentation matches the ground truth region $\mathbf{R}_i^{\mathcal{H}}$. The denominator normalizes the Jaccard index to the range $[0, 1]$.

For each human-automatic segmentation pair, a two-by-two comparison of all the respective regions is performed thanks to the Jaccard index. The resulting overall similarity measure is defined as

$$\mathrm{Sim}(\mathbf{S}^{\mathcal{H}}, \mathbf{S}^{\mathcal{A}}) = \frac{1}{\max\left(n^{\mathcal{H}}, n^{\mathcal{A}}\right)} \sum_{i=1}^{n^{\mathcal{H}}} \sum_{j=1}^{n^{\mathcal{A}}} J\left(\mathbf{R}_i^{\mathcal{H}}, \mathbf{R}_j^{\mathcal{H}}\right). \quad (20)$$

It ranges from near 0, meaning that the human and automatic segmentations are strongly different, to 1, meaning that the segmentations are identical.

The automatic segmentation results, shown in Figures 16, 17, and 18, are compared with each of the five available human segmentations thanks to the similarity measure. The mean values are displayed in Table 2, which shows that JSEG performs best on the *Plane* image. This table also shows that the sccf mode detection approach yields globally better results than the two tested classical methods for *Boat* and *Birds* images. Those quantitative results are consistent with the qualitative evaluation of the considered segmentations.

6. CONCLUSION

In this paper, color image segmentation has been considered as a pixel classification problem. Based on the detection of the modes of the 3D spatial-color compactness function (sccf), which describes the color image, our scheme consists in associating each homogeneous region with a mode of the sccf. This sccf yields the mode membership function of the fuzzy set "mode". A fuzzy morphological transformation, based on a combination of specific fuzzy erosions and dilations, is iteratively applied to this mode membership function. Fuzziness has been introduced in the morphological operators in order to take into account the local structure of the color point distribution in the color space. This enables to enhance the modes of the mode membership function, so that their detection becomes trivial. The pixels of the original color image are finally assigned to the classes associated with the identified modes.

We have shown the effectiveness of our approach by segmenting synthetic images which contain regions with strong overlapping color point distributions. These examples have also shown that our scheme can successfully handle nonequiprobable classes of pixels defined by nonglobular modes in the color space. Moreover, we have tested our approach with natural images in order to check that the simultaneous analysis of the spatial and color properties of the pixels is a relevant strategy for color image segmentation by pixel classification.

This work gives room to several possibilities for further improvement. First, the sccf is computed as the product of the homogeneity and the connectedness degrees. Other combinations, such as the sum or the maximum of these two degrees, could be considered to get a larger range of values. Second, another proposition concerns the evaluation of the structuring functions, which should integrate a compatibility measure between the mode membership degree of the considered color point and those of its adjacent color points. Indeed, the confidence in the assumption that a color point belongs to a mode (resp., a valley) is an increasing function of the number of its adjacent ones that also belong to a mode (resp., a valley). Third, other color spaces than (R, G, B) could be considered, since the performance of an image segmentation procedure is known to depend on the choice of the color space [36]. It would be interesting to study how the choice of a color space affects the representation of the color distribution by the sccf, and hence the shapes of the modes to be detected. A particular attention should be devoted to chromatic planes (u, v) and (H, S), which do not take the pixel intensity into account. The fourth point concerns the generalization of morphological operations, such as watershed, to fuzzy mode detection. Finally, it would be interesting to exploit the sccf to process color invariant features used by object recognition under changing illuminations.

REFERENCES

[1] H.-C. Chen, W.-J. Chien, and S.-J. Wang, "Contrast-based color image segmentation," *IEEE Signal Processing Letters*, vol. 11, no. 7, pp. 641–644, 2004.

[2] S. Di Zenzo, "A note on the gradient of a multi-image," *Computer Vision, Graphics, and Image Processing*, vol. 33, no. 1, pp. 116–125, 1986.

[3] A. Trémeau and N. Borel, "A region growing and merging algorithm to color segmentation," *Pattern Recognition*, vol. 30, no. 7, pp. 1191–1203, 1997.

[4] A. Trémeau and P. Colantoni, "Region adjacency graph applied to color image segmentation," *IEEE Transactions on Image Processing*, vol. 9, no. 4, pp. 735–744, 2000.

[5] H. Yan, "Color map image segmentation using optimized nearest neighbor classifiers," in *Proceedings of the 2nd IEEE International Conference on Document Analysis and Recognition (ICDAR '93)*, pp. 111–114, Tsukuba Science City, Japan, October 1993.

[6] T. Uchiyama and M. A. Arbib, "Color image segmentation using competitive learning," *IEEE Transactions on Pattern Analysis and Machine Intelligence*, vol. 16, no. 12, pp. 1197–1206, 1994.

[7] Y. W. Lim and S. U. Lee, "On the color image segmentation algorithm based on the thresholding and the fuzzy C-means techniques," *Pattern Recognition*, vol. 23, no. 9, pp. 935–952, 1990.

[8] J. Serra, *Image Analysis and Mathematical Morphology*, vol. 2 of *Theoretical Advances*, Academic Press, London, UK, 1988.

[9] L. Vincent and P. Soille, "Watersheds in digital spaces: an efficient algorithm based on immersion simulations," *IEEE Transactions on Pattern Analysis and Machine Intelligence*, vol. 13, no. 6, pp. 583–598, 1991.

[10] S. Dai and Y.-J. Zhang, "Color image segmentation with watershed on color histogram and Markov random fields," in *Proceedings of the 4th International Conference on Information, Communications & Signal Processing, and the 4th Pacific-Rim Conference on Multimedia (ICICS-PCM '03)*, vol. 1, pp. 527–531, Singapore, December 2003.

[11] H. Xue, T. Géraud, and A. Duret-Lutz, "Multiband segmentation using morphological clustering and fusion: application to color image segmentation," in *Proceedings of IEEE the International Conference on Image Processing (ICIP '03)*, vol. 1, pp. 353–356, Barcelona, Spain, September 2003.

[12] J. E. Cates, R. T. Whitaker, and G. M. Jones, "Case study: an evaluation of user-assisted hierarchical watershed segmentation," *Medical Image Analysis*, vol. 9, no. 6, pp. 566–578, 2005.

[13] Z. A. Aghbari and R. Al-Haj, "Hill-manipulation: an effective algorithm for color image segmentation," *Image and Vision Computing*, vol. 24, no. 8, pp. 894–903, 2006.

[14] C. Zhang, X. Zhang, M. Q. Zhang, and Y. Li, "Neighbor number, valley seeking and clustering," *Pattern Recognition Letters*, vol. 28, no. 2, pp. 173–180, 2007.

[15] Q. Ye, W. Gao, and W. Zeng, "Color image segmentation using density-based clustering," in *Proceedings of IEEE International Conference on Acoustics, Speech and Signal Processing (ICASSP '03)*, vol. 3, pp. 345–348, Hong Kong, April 2003.

[16] Y. Deng and B. S. Manjunath, "Unsupervised segmentation of color-texture regions in images and video," *IEEE Transactions on Pattern Analysis and Machine Intelligence*, vol. 23, no. 8, pp. 800–810, 2001.

[17] Y. Wang, J. Yang, and N. Peng, "Unsupervised color-texture segmentation based on soft criterion with adaptive mean-shift clustering," *Pattern Recognition Letters*, vol. 27, no. 5, pp. 386–392, 2006.

[18] Y.-G. Wang, J. Yang, and Y.-C. Chang, "Color-texture image segmentation by integrating directional operators into JSEG method," *Pattern Recognition Letters*, vol. 27, no. 16, pp. 1983–1990, 2006.

[19] F. Jing, M. Li, H.-J. Zhang, and B. Zhang, "Unsupervised image segmentation using local homogeneity analysis," in *Proceedings of IEEE International Symposium on Circuits and Systems (ISCAS '03)*, vol. 2, pp. 456–459, Bangkok, Thailand, May 2003.

[20] D. Comaniciu and P. Meer, "Mean shift: a robust approach toward feature space analysis," *IEEE Transactions on Pattern Analysis and Machine Intelligence*, vol. 24, no. 5, pp. 603–619, 2002.

[21] L. Macaire, N. Vandenbroucke, and J.-G. Postaire, "Color image segmentation by analysis of subset connectedness and color homogeneity properties," *Computer Vision and Image Understanding*, vol. 102, no. 1, pp. 105–116, 2006.

[22] C. Botte-Lecocq, O. Losson, and L. Macaire, "Color image segmentation by compacigram analysis," in *Proceedings of the 14th International Conference on Image Analysis and Processing Workshops (ICIAPW '07)*, pp. 212–215, Modena, Italy, September 2007.

[23] L. Busin, N. Vandenbroucke, L. Macaire, and J.-G. Postaire, "Colour space selection for unsupervised colour image segmentation by analysis of connectedness properties," *International Journal of Robotics and Automation*, vol. 20, no. 2, pp. 70–77, 2005.

[24] M. R. Hamid, A. Baloch, A. Bilal, and N. Zaffar, "Object segmentation using feature based conditional morphology," in *Proceedings of the 12th International Conference on Image Analysis and Processing (ICIAP '03)*, pp. 548–553, Mantova, Italy, September 2003.

[25] J.-G. Postaire, R. D. Zhang, and C. Lecocq-Botte, "Cluster analysis by binary morphology," *IEEE Transactions on Pattern Analysis and Machine Intelligence*, vol. 15, no. 2, pp. 170–180, 1993.

[26] S. H. Park, I. D. Yun, and S. U. Lee, "Color image segmentation based on 3D clustering: morphological approach," *Pattern Recognition*, vol. 31, no. 8, pp. 1061–1076, 1998.

[27] R.-D. Zhang and J.-G. Postaire, "Convexity dependent morphological transformations for mode detection in cluster analysis," *Pattern Recognition*, vol. 27, no. 1, pp. 135–148, 1994.

[28] C. Botte-Lecocq, K. Hammouche, A. Moussa, J.-G. Postaire, A. Sbihi, and A. Touzani, "Image processing techniques for unsupervised pattern classification," in *Scene Reconstruction, Pose Estimation and Tracking*, pp. 357–378, ARS Publications, Vienna, Austria, 2007.

[29] L. Shafarenko, M. Petrou, and J. Kittler, "Automatic watershed segmentation of randomly textured color images," *IEEE Transactions on Image Processing*, vol. 6, no. 11, pp. 1530–1544, 1997.

[30] R. M. Haralick, S. R. Sternberg, and X. Zhuang, "Image analysis using mathematical morphology," *IEEE Transactions on Pattern Analysis and Machine Intelligence*, vol. 9, no. 4, pp. 532–550, 1987.

[31] A. Gillet, L. Macaire, C. Botte-Lecocq, and J.-G. Postaire, "Color image segmentation by analysis of 3D histogram with fuzzy morphological filters," in *Fuzzy Filters for Image Processing-Studies in Fuzziness and Soft Computing*, pp. 154–177, Springer, New York, NY, USA, 2002.

[32] I. Bloch and H. Maître, "Fuzzy mathematical morphologies: a comparative study," *Pattern Recognition*, vol. 28, no. 9, pp. 1341–1387, 1995.

[33] D. Martin, C. Fowlkes, D. Tal, and J. Malik, "A database of human segmented natural images and its application to evaluating segmentation algorithms and measuring ecological statistics," in *Proceedings of the 8th IEEE International Conference on Computer Vision (ICCV '01)*, vol. 2, pp. 416–423, Vancouver, BC, Canada, July 2001.

[34] P. Vannoorenberghe and G. Flouzat, "A belief-based pixel labeling strategy for medical and satellite image segmentation," in *Proceedings of IEEE International Conference on Fuzzy Systems*, pp. 1093–1098, Vancouver, BC, Canada, July 2006.

[35] F. Ge, S. Wang, and T. Liu, "A new benchmark for image-segmentation evaluation," *Journal of Electronic Imaging*, vol. 16, no. 3, Article ID 033011, 16 pages, 2006.

[36] N. Vandenbroucke, L. Macaire, and J.-G. Postaire, "Color image segmentation by pixel classification in an adapted hybrid color space. Application to soccer image analysis," *Computer Vision and Image Understanding*, vol. 90, no. 2, pp. 190–216, 2003.